

PAPER



Cite this: *New J. Chem.*, 2019, 43, 5518

Rapid and efficient electrochemical synthesis of a zinc-based nano-MOF for Ibuprofen adsorption†

Otávio José de Lima Neto, ^a Allana Christina de Oliveira Frós, ^a
Bráulio Silva Barros, ^{*b} Arthur Felipe de Farias Monteiro ^a and
Joanna Kulesza ^{*a}

In this paper, mixed-ligand Zn-based metal–organic framework [Zn(1,3-bdc)_{0.5}(bzim)] was synthesized via the electrochemical method. Studies on different synthesis parameters demonstrated that the time of reaction and the current density were the most significant factors affecting the purity and yield of the product. We found that the best conditions to obtain pure-phase MOF with high yield (87%) were a 60 mA current and a 2 h reaction time. The applied synthesis conditions allowed the reaction time and size of the crystallites to be significantly reduced when compared to the conventional solvothermal, hydrothermal or diffusion methods. The most promising sample was fully characterized by Powder X-ray Diffraction (PXRD), Infrared Spectroscopy (FTIR), Scanning Electron Microscopy (SEM), Thermogravimetry (TG), and surface area measurement (BET). The electrochemically synthesized pure-phase sample was tested for the adsorption of a model analgesic and anti-inflammatory drug, Ibuprofen, which was quantified by UV-Vis and ¹³C NMR spectroscopy. The presence of the drug loaded on the material was also verified by FTIR, TG, SEM, and BET analyses.

Received 19th December 2018,
Accepted 12th March 2019

DOI: 10.1039/c8nj06420b

rsc.li/njc

Introduction

Metal–organic frameworks (MOFs) are hybrid materials structurally based on metal ions or clusters and polytopic organic ligands which are interconnected forming 2D or 3D porous structures. In the last two decades, research on MOFs has received much attention because of the increasing number of applications for these materials in gas storage and separation,¹ catalysis,² sensors,³ imaging,⁴ drug delivery⁵ and many others. Importantly, especially for biomedical applications, the size of MOF particles must be reduced to the nanoscale regime in order to reach high viability for practical applications. Moreover, it is well known that nano-MOFs present different or at least enhanced properties compared to bulk materials due to the high surface-to-volume ratio and quantum size effects.⁶ The size requirements cannot be frequently achieved by using conventional synthetic routes such as hydrothermal and solvothermal methods or the slow diffusion approach. Also, the conventional routes have some limitations on scaling up. Therefore, alternative approaches such as the microwave assisted

method, and sonochemical and electrochemical methods have also been successfully introduced.

The electrochemical method presents many advantages over other approaches such as mild reaction conditions (commonly performed at ambient temperature and pressure), short reaction time (up to 2 hours), high yields, low-energy consumption, simple operation, and no need of using special equipment.⁷ Pioneered by researchers from BASF in 2005,⁸ anodic dissolution has become the most common electrochemical method for MOF preparation, mainly those based on Cu²⁺,^{8–11} Co²⁺,¹² Zn²⁺,^{11–16} Ni²⁺,¹⁷ and Al³⁺.¹¹ In this approach, metal cations are produced *in situ* by anodic oxidation, which eliminates the use of troublesome counterions such as nitrates or chlorates, and thus, facilitates the synthesis control. It has been demonstrated that electrochemical parameters such as supporting electrolyte and current density play an important role in tuning the morphology (size, shape, and distribution of particles) and the yield of the reaction.^{9,15} Despite the attractive features exhibited by this method, the electrochemically synthesized MOFs are still rare compared to materials prepared by using other methods and systematic studies on the effects of the electrochemical parameters on product formation are still needed.

In this work, [Zn(1,3-bdc)_{0.5}(bzim)] nano-MOF has been synthesized using the electrochemical method, and a detailed study of the most important variables governing the electrochemical synthesis of MOFs is presented. The influence of

^a Departamento de Química Fundamental, Universidade Federal de Pernambuco, Av. Prof. Moraes Rego, 1235 - Cidade Universitária, 50670-901 Recife, PE, Brazil.
E-mail: joanna.kulesza@ufpe.br

^b Departamento de Engenharia Mecânica, Universidade Federal de Pernambuco, Av. Prof. Moraes Rego, 1235 - Cidade Universitária, 50670-901 Recife, PE, Brazil.
E-mail: braulio.barros@ufpe.br

† Electronic supplementary information (ESI) available. See DOI: 10.1039/c8nj06420b

three factors (current, time of reaction and quantity of supporting electrolyte) on the yield, purity and crystallite size of the product was evaluated. The pure-phase sample was tested for the adsorption of a model analgesic and anti-inflammatory drug, Ibuprofen, which was quantified by UV-Vis and confirmed by ^{13}C NMR spectroscopy.

Experimental

Materials

All reagents and solvents were purchased from commercial suppliers and used without further purification. Sodium nitrate (NaNO_3 – 99%) was provided by Vetec. Ibuprofen sodium salt (Na-IBU – 99%, $\text{MM } 228.29 \text{ g mol}^{-1}$), isophthalic acid (1,3- H_2BDC – 99%) and benzimidazole (Hbzim – 98%) were acquired from Sigma Aldrich. Zinc plates ($70 \times 10 \text{ cm}$) from Ilca were used as an electrode material. Solvents: N,N -dimethylformamide (DMF-PA) and ethanol (EtOH-PA) were purchased from Dinâmica. 1,4-Dioxane (99%) and CDCl_3 (99.9%) used for NMR measurements were purchased from Sigma Aldrich.

Equipment and characterization

Electrochemical syntheses were performed under constant current or voltage using a Micken DC power supply PS-1502DD+ and a HIKARI multimeter HM-1000. Powder X-ray diffraction patterns were recorded on a Bruker D2 Phaser using $\text{CuK}\alpha$ ($\lambda = 1.5406 \text{ \AA}$) radiation with a Ni filter, at a voltage of 30 kV and 10 mA. Experiments were conducted at 2θ values ranging from 3 to 70° with a step of 0.02° . For the calculations of the crystallite size, the most intense peak of the XRD patterns of $[\text{Zn}(1,3\text{-bdc})_{0.5}(\text{bzim})]$ at $2\theta = 7.85^\circ$ was chosen. The simulated XRD pattern was obtained using the program Mercury 3.8. Thermogravimetric analyses (TGA) were performed using a Shimadzu DTG-60H thermal analysis system. Samples were heated from 20°C to 900°C at a rate of $10^\circ\text{C min}^{-1}$ in a continuous nitrogen flow atmosphere. Fourier transform infrared (ATR-FTIR) experiments were carried out on a Bruker Vertex 70/v spectrometer in the range of $4000\text{--}400 \text{ cm}^{-1}$. Morphological analyses and images were acquired on a Scanning Electron Microscope (SEM), model Tescan Mira 3. The surface area

was measured from BET adsorption isotherms of N_2 using a Quantachrome apparatus model Nova 3200e. UV-Vis spectra of Ibuprofen were recorded on a PerkinElmer Lambda 650 spectrophotometer in the range of 500–240 nm. ^{13}C NMR spectra of Ibuprofen were acquired on an NMR spectrometer (Agilent 300 MHz). Typically, 10 000 scans were collected into 32 K memory data points with a relaxation delay of 20 s and an acquisition time of 1.39 s. The integrations were computed according to the GSD protocol¹⁸ using Mnova 11.04 software.

Electrochemical synthesis of $[\text{Zn}(1,3\text{-bdc})_{0.5}(\text{bzim})]$

The synthesis of $[\text{Zn}(1,3\text{-bdc})_{0.5}(\text{bzim})]$ was first reported by Cui *et al.*¹⁹ and later by our group²⁰ (see the ESI,† Fig. S1). Nevertheless, the hydrothermal,¹⁹ solvothermal²⁰ and slow diffusion²⁰ methods provided the material in only low to moderate yields, 23.0, 45.4 and 41.6%, within long reaction time, 8.5, 8 and 14 days, respectively. In this work, $[\text{Zn}(1,3\text{-bdc})_{0.5}(\text{bzim})]$ was synthesized by the electrochemical method. Initially, 8 syntheses (T1–T7) were carried out using the following levels of electrochemical variables: time of reaction, T (1 h, 1.5 h or 2 h), quantity of electrolyte, Q (112, 156 or 200 mg) and current, C (40, 60 or 80 mA) to evaluate the influence of these parameters on the phase purity, crystallite size and yield of products (Table 1).

Typically, 2 mmol (332 mg) of 1,3- H_2bdc and 1 mmol (118 mg) of Hbzim were dissolved in 30 mL of DMF/EtOH mixture (15/15 mL). Separately, an aqueous solution of the supporting electrolyte (NaNO_3) was prepared in 15 mL of distilled water and then added to the reaction mixture. Subsequently, two zinc electrodes (previously polished with sand paper and washed with ethanol) were suitably placed in a polymer lid in such a way that 2.5 cm of the plates were immersed in the reaction mixture and apart from each other by 1.5 cm. A DC power supply was then connected to the electrodes, and the voltage was adjusted to keep the current constant at the levels as shown in Table 1. All the tests were performed at room temperature and with stirring during 1, 1.5 or 2 h. At the end of the reaction, the white powder formed in the electrode surface and solution was carefully isolated, filtered, washed with DMF and distilled water, and dried at

Table 1 Summary of synthesis parameters employed for the preparation of $[\text{Zn}(1,3\text{-bdc})_{0.5}(\text{bzim})]$

Sample	Time of reaction, T [h]	Quantity of electrolyte, Q [mg]	Current, C [mA]	Voltage, V [V]	No. of Zn^{2+} [mmol]	Yield of reaction [%]	Crystallite size [nm]
T1	2	112	40	6.0–6.5	1.49	0.0	ND
T2	2	200	40	4.0–4.2	1.49	43.6 ^a	105.9
T3	1	112	80	10.5–12.0	1.49	11.2	ND
T4	2	112	80	12.3–15.2	2.98	160.8 ^a	69.8
T5	1	200	80	7.5–7.9	1.49	9.9	ND
T6	2	200	80	8.4–13.0	2.98	212.6 ^a	106.0
T7	1.5	156	60	5.4–6.4	1.68	73.4	27.5
T8	2	156	60	6.1–6.5	2.24	87.0	32.3
T9	2	200	65–70	8.0	2.61	138.2 ^a	69.8
T10	2	200	70–80	10.0	2.98	159.5 ^a	238.8
T11	2	200	80	6.7–7.1	2.24	ND ^b	ND
RT ^c	14 days	—	—	—	2.00	41.6	61.5
ST ^c	8 days	—	—	—	2.00	45.4	72.1

ND – not determined, ^a Presence of two or more phases. ^b Molar ratio 1,3- H_2bdc :Hbzim, 1:0. ^c Barros *et al.*²⁰

60 °C for 2 h. After the evaluation of the effect of the variables (C , Q , and T) on the phase purity and yield, another synthesis (T8) was performed under the same synthesis conditions as T7 but with the time of reaction increased to 2 h. Additionally, two syntheses with the fixed voltage at 8 V (T9) and 10 V (T10) and the synthesis without the presence of benzimidazole (T11) were performed.

Drug adsorption experiments

Adsorption tests were conducted as follows: 20 mg of the adsorbent (T8) were immersed in 1 mL of Ibuprofen ethanolic solution (30 mg mL⁻¹ of Na-IBU), and the resulting suspension was stirred during 1 day in a 5 mL glass sealed tube carefully protected against luminosity due to the drug photosensitivity. The system without the adsorbent (blank experiment) was also conducted under the same conditions. Afterward, the supernatant was separated from the solid material by centrifugation (6000 rpm, 10 minutes) and the solution was analyzed by two different methods, UV-Vis spectrophotometry and ¹³C NMR spectroscopy, to determine the rest of the unloaded Ibuprofen.

For the quantification by the UV-Vis method, three aliquots of 40 μL were withdrawn from the centrifuged supernatant solution and placed in three tubes (5 mL) each containing 3 mL of ethanol. The same procedure was carried out for the blank experiment. The quantity of the drug adsorbed on the material (mgIBU/gMOF) was calculated according to eqn (1). The concentrations of IBU in the sample and blank experiments were obtained using a calibration curve equation (see details in the ESI,† Fig. S2).

$$\text{mgIBU/gMOF} = \frac{\{[\text{BC}] - [\text{SC}]\} \times D_f}{m_{\text{MOF}} \times V} \times 1000 \quad (1)$$

where: BC is the concentration of IBU in the blank experiment (mg mL⁻¹), SC is the concentration of IBU in the sample experiment (mg mL⁻¹), D_f is the dilution factor, V is the solution volume, and m_{MOF} is the amount of MOF used in the adsorption tests.

For the IBU quantification by ¹³C NMR, 500 μL of the IBU centrifuged solution were transferred to a 5 mm NMR tube, and 300 μL of the internal standard solution (1,4-dioxane) dissolved in CDCl₃ (600 μL) were added. The same procedure was used for the blank experiment.

The adsorbed amount of Ibuprofen was calculated from eqn (2):

$$\text{mgIBU/gMOF} = \frac{\Delta I_{\text{IBU}}}{I_{\text{ref}}} \frac{N_{\text{ref}}}{N_{\text{IBU}}} \frac{MM_{\text{IBU}}}{m_{\text{MOF}}} \times 1000 \quad (2)$$

where, ΔI_{IBU} is the difference of the integral in the spectrum before (I_{x1}) and after the adsorption (I_{x2}), I_{ref} and n_{ref} are the integral value and number of mol, respectively, of 1,4-dioxane (reference), N is the number of carbon nuclei corresponding to the signal of IBU or reference, MM_{IBU} is the molar mass of IBU, and m_{MOF} is the amount of MOF used in the adsorption test.

All details including ¹³C NMR spectra and calculations are placed in the ESI† (Fig. S3 and S4 and Table S1).

All adsorption experiments were carried out in triplicate. The integration area corresponds to the average of the repetition of ten times of the integrals measured (error <1%), and the absorbance is the average of three repetitions.

Results and discussion

Electrosynthesis of [Zn(1,3-bdc)_{0.5}(bzim)]

The careful analysis of data from Table 1 led to the conclusion that only two variables, time of reaction (T) and current (C), had a significant influence on the yield of the reaction, whereas the quantity of supporting electrolyte (Q) did not have a significant influence on this response. Although the quantity of Zn²⁺ ions produced during the synthesis T1 was sufficient for the formation of [Zn(1,3bdc)_{0.5}(bzim)], no product was obtained. This fact may be explained by the low conductivity of the solution. By increasing the electrolyte concentration, the conductivity was increased, which resulted in higher yields (43.6% for T2). The increased conductivity improves the yield because less energy is thus required to overcome the Ohmic drop in the solution and can, therefore, be used to dissolve the electrode. The conditions of the highest level of current (80 mA) and the time of reaction (2 h) drastically increased the quantity of the product (T4 and T6). As expected, the increased conductivity in the case of T6 compared to T4, increased the yield of the reaction. One can notice, however, that the yield of the reaction was higher than 100% in both cases, which can indicate the formation of two or more phases and this was posteriorly confirmed by XRD studies. When the time of reaction was shortened to 1 h, the yield of the product was very low, 11.22 and 9.89, for T3 and T5, respectively. In these cases, the increased conductivity did not influence the yield of the reaction. Thus, one can conclude that the time of reaction and current (and their interactions) influenced the yield of the product the most. A T7 test was conducted to optimize the synthesis conditions. In this test, the intermediate levels of the three factors were applied (the time of reaction 1.5 h, the quantity of electrolyte 156 mg, current 60 mA). These conditions furnished the desired product in 73.4% yield. To further increase the yield of the product, the time of reaction was increased to 2 h (T8) maintaining the other two factors at the same level as in T7. This combination of factors furnished the product in 87% yield. This yield is much higher than that reported by Cui *et al.* (23%)¹⁹ or previously by our group (41.6 and 45.4% for RT and ST, respectively).²⁰ Two syntheses performed at constant voltages T9 and T10 led to the formation of secondary phases (yield higher than 100%) posteriorly confirmed by PXRD analysis. To keep the voltage constant at 8 and 10 V, the current changed between 65–70 mA and 70–80 mA for T9 and T10, respectively. These values of current, higher than 60 mA, might have promoted the formation of secondary phases as observed in current-constant syntheses.

X-ray diffraction analysis

Fig. 1 shows the powder diffraction patterns of samples T2, T4, T6, T7, T8, T9, and T10, as well as the simulated pattern

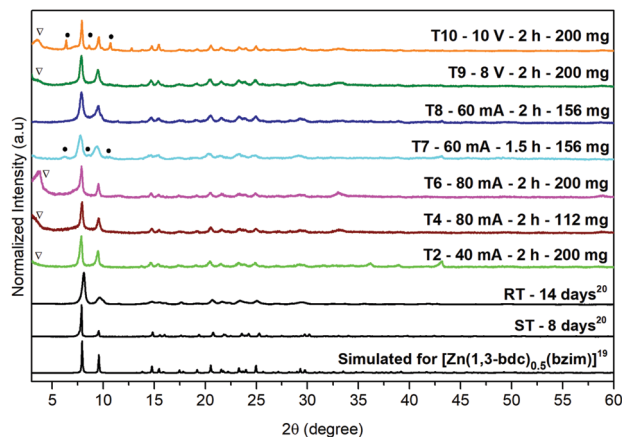


Fig. 1 PXRD patterns of obtained samples T2, T4, T6, T7, T8, T9, and T10 and the simulated one from the single crystal data of $[\text{Zn}(\text{1,3-bdc})_{0.5}(\text{bzim})]^{19}$ compared to PXRD patterns of the products obtained by the solvothermal and room temperature methods.²⁰ Syntheses T1, T3, and T5 did not produce a sufficient quantity of product for this analysis.

generated from the CIF file COD no 2213328.¹⁹ It can be seen that the desired phase of $[\text{Zn}(\text{1,3-bdc})_{0.5}(\text{bzim})]$ crystallized during all synthesis conditions tested. However, only the pattern of the sample T8 presents a single-phase. Although the synthesis conditions of T7 were similar to that of T8, the presence of the secondary phase in the PXRD pattern of T7 may be evidenced (marked with a filled circle, phase not identified). It appears that the formation of the MOF $[\text{Zn}(\text{1,3-bdc})_{0.5}(\text{bzim})]$ occurs *via* the crystallization of an intermediate with a subsequent phase-transformation completed only after two hours of reaction. The same intermediate phase was found in the pattern of T10 (synthesis performed at a constant voltage of 10 V).

Samples prepared within 2 h under a current of 40 or 80 mA (T2, T4, and T6) and those prepared under constant voltage (T9 and T10) present a broad peak below 5° (2θ). Curiously, this peak appears in a variable position depending on the synthesis conditions, which can be associated with the variation of the unit cell size of the structure. Hirai *et al.* have reported the formation of layered zinc hydroxides (Zn-LDH) stabilized by intercalated terephthalate molecules (TPA).²¹ Three types of Zn-LDH were identified with different interlayer distances according to the amount of TPA molecules intercalated in these structures. As a result, a peak related to this phase was shifted as a function of the size of the unit cell.²¹ Thus, in our work, we suggest that because isophthalic acid was used in excess, the secondary phases containing isophthalate might have been formed.

To estimate the composition of the secondary phases, the synthesis in the absence of benzimidazole was performed (T11). In the PXRD pattern of T11 (Fig. S5, ESI[†]), peaks at about 6.4° , 7.10° and 10.5° coincide with the peaks found in sample T10 and less intense in T7. Also, the peak at a low angle at about $2\theta = 3.0^\circ$ can be observed. The same peak appeared in samples T2 and T4, and was more shifted in sample T6, as well as in samples conducted under constant voltage (T9 and T10). This observation indicates that the secondary phases in those

samples do not contain benzimidazole and most probably are associated with Zn-isophthalate hybrid materials.

Crystallite size

The electrochemical synthesis afforded nano MOFs with a crystallite size in the range of 27.5–238.8 nm (see Table 1). Samples T7 and T8 present the smallest and very similar crystallite size, 27.5 and 32.3 nm, respectively, both prepared under intermediate current (60 mA) and electrolyte quantity (156 mg) but different synthesis time (1.5 and 2 h, for T7 and T8, respectively). Slightly bigger crystallite size in the case of sample T8 might have been caused by the longer reaction time. For the rest of the samples, the crystallite size is at least two times (for T4 and T9) or three times bigger (for T2, T6) than that observed for T8, which may be related to the presence of the secondary phase in these samples. Sample T10, for which at least two different secondary phases were found, presents the largest crystallite size (238.8 nm).

Worth noting is the fact that the reference samples prepared by the slow diffusion method at room temperature and the solvothermal method present larger crystallite size (61.50 nm and 72.1 nm, respectively) than that of the pure-phase sample T8 (32.3 nm) indicating that the electrochemical method is more efficient in reducing the crystallite size of a MOF sample. This fact may be explained by the greater control over the concentration of metal ions during the electrochemical synthesis. In general, rapid dissolution increases the metal ion concentration, which affords fast nucleation and consequently smaller crystals.

TGA

Thermal stability of the electrochemically synthesized pure-phase sample T8 was investigated by thermogravimetric analysis (TGA), and the results were compared to those of the previously reported sample prepared by the solvothermal method (ST).²⁰ The thermogravimetric profiles of both samples are similar to each other (Fig. 2), and present two-step weight loss corresponding to the decomposition of the carboxylate and benzimidazolate part of the framework.

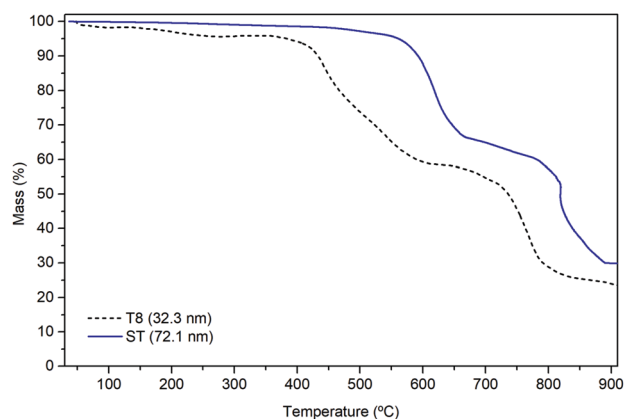


Fig. 2 TG curves of the samples T8 and ST.²⁰

The two samples, however, starts to decompose in very distinct temperatures. Whereas the reference sample is stable up to 472 °C, sample T8 starts to collapse at a much lower temperature (347 °C). The lower thermal stability of the sample T8 is related to the smaller particle size (32.3 nm) compared to the ST sample (72.1 nm). Since nanoscale materials have higher surface-to-volume ratio compared to bulk materials and more “matter” is exposed to the environment, they tend to be thermodynamically unstable because the surface atoms are more energetic than those from the volume.^{6,22}

Adsorption of Ibuprofen onto [Zn(1,3-bdc)_{0.5}(bzim)]

In the field of drug loading and release, MOFs have been shown as promising host systems. Férey *et al.* reported for the first time the use of a porous material MOF (MIL101-Fe) to incorporate Ibuprofen for controlled release.²³ Since then, studies on drug loading capacity, and kinetic release with the use of diverse frameworks including Zn-based MOFs^{16,24} have been reported. In this work, [Zn(1,3-bdc)_{0.5}(bzim)] was tested for Ibuprofen loading capacity. Sample T8 was chosen for drug adsorption tests due to the highest yield and purity among all synthesized samples. The Ibuprofen sodium salt was adsorbed by the sample from a solution of ethanol, and the adsorbed amount was quantified by UV/Vis spectroscopy and confirmed by ¹³C NMR spectroscopy.

X-Ray powder diffraction performed on both materials T8 and IBU@T8 (before and after adsorption, respectively) proved that the structure is retained after the drug adsorption (see Fig. S6, ESI†). The presence of the adsorbed Ibuprofen was confirmed by FT-IR spectroscopy, Thermogravimetric analysis (TGA), Scanning Electron Microscopy (SEM) and N₂ adsorption experiments.

The FT-IR spectrum of T8 presents some changes after drug loading (Fig. 3a); however, the structure of the framework maintained its integrity, which is consistent with the PXRD analyses.

The change in the relative intensity of the bands corresponding to the two asymmetric vibration modes of COO⁻ of the framework may be observed. New bands at 1698 cm⁻¹ and in the region between 2796 and 3642 cm⁻¹, corresponding to the

COO⁻ and the C–H groups, respectively, of the Ibuprofen salt, are visible in the FT-IR spectrum of IBU@T8. Both bands are also present in the spectrum of the free anionic Ibuprofen. Also, a set of bands at 1609, 1464, 1063, 889 and 586 cm⁻¹ highly consistent with those of free Ibuprofen, can also be observed in the IR spectrum of IBU@T8. The band at 1655 cm⁻¹ associated with the presence of DMF molecules in the framework is absent in the FT-IR spectrum of IBU@T8 suggesting that drug molecules might have expelled solvent molecules from the structure. The IR results indicate the presence of Ibuprofen molecules in the drug-loaded T8. We believe that the interactions between drug molecules and the framework are mostly governed by π - π interactions between the aromatic rings of Ibuprofen and the ligands in the framework. This assumption may be supported by the observation of the band shift at *ca.* 1500 cm⁻¹ corresponding to the benzimidazole stretching mode, which may indicate the contribution of the benzimidazole ring in the framework-drug interactions. Since the dimensions of the pores in the structure of [Zn(1,3-bdc)_{0.5}(bzim)] (5.9 Å × 5.0 Å) are much smaller compared to those of Ibuprofen (6 Å × 9.4 Å),²⁵ the adsorption may have occurred mostly on the surface of the material.

Thermogravimetric curves of T8, IBU, and IBU@T8 samples are compared in Fig. 3b. Four weight losses can be observed within the range 22–100 °C (I), 160–400 °C (II), 400–600 °C (III) and 600–775 °C (IV) for the IBU@T8 sample. The first two losses correspond to the departure of water and Ibuprofen, respectively, which is consistent with the results for the MIL53-IBU sample reported by Férey *et al.*²⁶ No weight loss corresponding to the DMF molecules was found, which is consistent with the FT-IR results. Above 400 °C, the two losses are associated with the two-step destruction of the framework as well as possible traces of Ibuprofen. At temperatures higher than 400 °C, the distinction of the weight losses is more complex due to the drug and the framework decomposition at the same time.

Fig. 4 presents micrographs of the MOF loaded with Ibuprofen IBU@T8 compared to the T8 sample before adsorption. The powder of the T8 sample is composed of small particles assembled into soft micrometric porous sponge-like agglomerates (Fig. 4a).

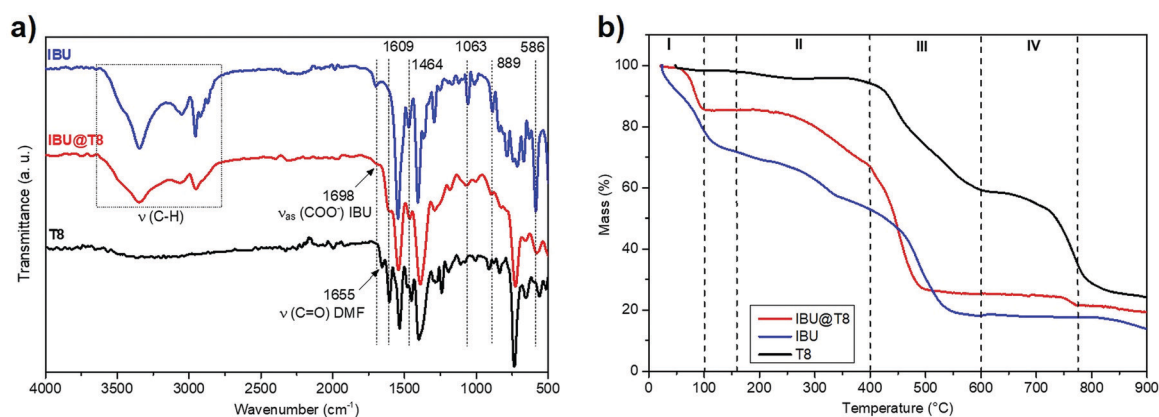


Fig. 3 FT-IR (a) and TGA (b) of the framework with Ibuprofen loaded (IBU@T8) compared to free IBU and T8 before adsorption.

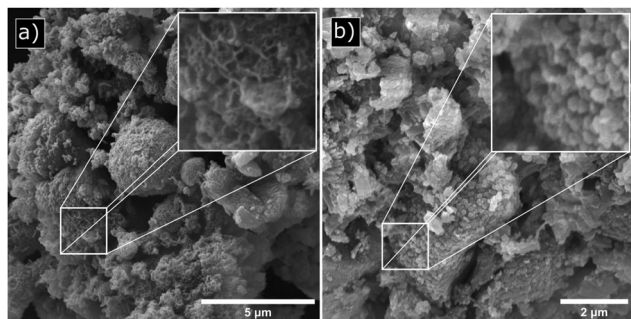


Fig. 4 Micrographs of the sample T8 before adsorption (a) and Ibuprofen loaded MOF (IBU@T8) (b).

The sample IBU@T8 presents different morphology of the drug-free sample. The morphological analysis of IBU@T8 revealed the presence of quasi-spherical particles smaller than 500 nm on the surface of the micrometric blocks, which may indicate that Ibuprofen has been attached to the surface of the agglomerates.

The sample T8 $[\text{Zn}(1,3\text{-bdc})_{0.5}(\text{bzim})]$ shows a reversible Type-II isotherm of N_2 adsorption/desorption which is typical for a macroporous adsorbent²⁷ (see Fig. S8, ESI[†]) and a surface area of $14.404 \text{ m}^2 \text{ g}^{-1}$. Such behavior is expected since the $[\text{Zn}(1,3\text{-bdc})_{0.5}(\text{bzim})]$ possesses clipped structural pores, with little accessible surface or pore volume. On the other hand, the presence of inter-grain macropores can be observed from the SEM image (Fig. 4a). N_2 adsorption/desorption isotherms after Ibuprofen loading are similar to the pure sample; however, the BET surface area was $8.036 \text{ m}^2 \text{ g}^{-1}$. This decrease of 45% might confirm the crystallization of the Ibuprofen molecules mostly on the surface of the adsorbent.

The UV-Vis studies showed that the material adsorbed 163.9 mg g^{-1} of Ibuprofen, which was similar to the value obtained by ^{13}C NMR spectroscopy (160.7 mg g^{-1}). This value is lower than those obtained for large-cage frameworks such as MIL-100 and MIL-101 (347 and 1376 mg , respectively).²⁸ On the other hand, the synthesized material exhibited higher Ibuprofen uptake than another MOF from the MIL family, MIL-53 (104 mg for 1 day).²⁶ The significant uptake of the drug by $[\text{Zn}(1,3\text{-bdc})_{0.5}(\text{bzim})]$ may be governed by the hydrophobic feature of the framework, which is compatible with the hydrophobic nature of Ibuprofen.

Conclusions

In this work, the mixed-ligand metal-organic framework $[\text{Zn}(1,3\text{-bdc})_{0.5}(\text{bzim})]$ was successfully synthesized *via* the electrochemical method for the first time. It was found that the time of reaction and current were the most significant factors affecting the purity and the yield of the desired product. The appropriate selection of the synthesis conditions (time of reaction, 2 h and current of 60 mA) allowed us to obtain pure-phase desired nano-MOF (crystallite size of 32.3 nm) in a much higher yield (87%) than previously reported hydrothermal, solvothermal or slow diffusion methods. Moreover, the time of reaction was shortened from at least 8 days (solvothermal method) to only 2 h. The preliminary UV-Vis studies showed that the material adsorbed a significant

amount of Ibuprofen (163.9 mg g^{-1}), which was similar to the value obtained by ^{13}C NMR spectroscopy (160.7 mg g^{-1}).

Conflicts of interest

There are no conflicts to declare.

Acknowledgements

The students thank FACEPE (O. J. L. N.) and CNPq (A. C. O. F. and A. F. F. M.) for a scholarship granted. This work was financially supported by CNPq and FACEPE (Grants no. 403747/2016-3, APQ-0675-1.06/14, APQ-0818-1.06/15). The authors thank – LabSMaC (Laboratório de Síntese de Materiais Cerâmicos/UFCG) for N_2 adsorption experiments.

References

- H. Li, K. Wang, Y. Sun, C. T. Lollar, J. Li and H. C. Zhou, *Mater. Today*, 2018, **21**, 108–121.
- Y. B. Huang, J. Liang, X. S. Wang and R. Cao, *Chem. Soc. Rev.*, 2017, **46**, 126–157.
- F.-Y. Yi, D. Chen, M.-K. Wu, L. Han and H.-L. Jiang, *ChemPlusChem*, 2016, **81**, 675–690.
- M. A. Chowdhury, *ChemBioEng Rev.*, 2017, **4**, 225–239.
- C.-Y. Sun, C. Qin, X.-L. Wang and Z.-M. Su, *Expert Opin. Drug Delivery*, 2013, **10**, 89–101.
- B. S. Barros, O. J. de Lima Neto, A. C. de Oliveira Frós and J. Kulesza, *ChemistrySelect*, 2018, **3**, 7459–7471.
- H. Al-Kutubi, J. Gascon, E. J. R. Sudhölter and L. Rassaei, *ChemElectroChem*, 2015, **2**, 462–474.
- U. Mueller, M. Schubert, F. Teich, H. Puetter, K. Schierle-Arndt and J. Pastré, *J. Mater. Chem.*, 2006, **16**, 626–636.
- R. Senthil Kumar, S. Senthil Kumar and M. Anbu Kulandainathan, *Microporous Mesoporous Mater.*, 2013, **168**, 57–64.
- J. Kulesza, B. S. Barros, I. M. V. da Silva, G. G. da Silva and S. Alves Júnior, *CrystEngComm*, 2013, **15**, 8881–8882.
- A. Martinez Joaristi, J. Juan-Alcañiz, P. Serra-Crespo, F. Kapteijn and J. Gascon, *Cryst. Growth Des.*, 2012, **12**, 3489–3498.
- Z. Li, J. Cui, Y. Liu, J. Li, K. Liu and M. Shao, *ACS Appl. Mater. Interfaces*, 2018, **10**, 34494–34501.
- H. Yang, X. Liu, X. Song, T. Yang, Z. Liang and C. Fan, *Trans. Nonferrous Met. Soc. China*, 2015, **25**, 3987–3994.
- W. L. H. Yang, H. Du, L. Zhang and Z. Liang, *Int. J. Electrochem. Sci.*, 2015, **10**, 1420–1433.
- D. N. S. Khazalpour, V. Safarifard and A. Morsali, *RSC Adv.*, 2015, **5**, 36547–36551.
- W. W. Lestari, M. Arvinawati, R. Martien and T. Kusumaningsih, *Mater. Chem. Phys.*, 2018, **204**, 141–146.
- W. W. Lestari, I. D. Winarni and F. Rahmawati, *IOP Conf. Ser.: Mater. Sci. Eng.*, 2017, **172**, 1–9.
- M. A. Bernstein, S. Sýkora, C. Peng, A. Barba and C. Cobas, *Anal. Chem.*, 2013, **85**, 5778–5786.
- Y.-C. Cui, J.-J. Wang, B. Liu, G.-G. Gao and Q.-W. Wang, *Acta Crystallogr., Sect. E: Struct. Rep. Online*, 2007, **63**, m1204–m1205.

- 20 B. S. Barros, J. Chojnacki, A. A. Macêdo Soares, J. Kulesza, L. Lourenço Da Luz and S. A. Júnior, *Mater. Chem. Phys.*, 2015, **162**, 364–371.
- 21 Y. Hirai, K. Furukawa, H. Sun, Y. Matsushima, K. Shito, A. Masuhara, R. Ono, Y. Shimbori, H. Shiroishi, M. S. White and T. Yoshida, *Microsyst. Technol.*, 2018, **24**, 699–708.
- 22 G. Sargazi, D. Afzali and A. Mostafavi, *Ultrason. Sonochem.*, 2018, **41**, 234–251.
- 23 P. Horcajada, C. Serre, M. Vallet-Regí, M. Sebban, F. Taulelle and G. Férey, *Angew. Chem., Int. Ed.*, 2006, **45**, 5974–5978.
- 24 N. Motakef-Kazemi, S. A. Shojaosadati and A. Morsali, *J. Iran. Chem. Soc.*, 2016, **13**, 1205–1212.
- 25 B. N. Bhadra, I. Ahmed, S. Kim and S. H. Jhung, *Chem. Eng. J.*, 2017, **314**, 50–58.
- 26 P. Horcajada, C. Serre, G. Maurin, N. A. Ramsahye, F. Balas, M. Vallet-Regí, M. Sebban, F. Taulelle and G. Férey, *J. Am. Chem. Soc.*, 2008, **130**, 6774–6780.
- 27 K. S. W. Sing, *Pure Appl. Chem.*, 1982, **54**, 2201–2218.
- 28 P. Horcajada, C. Serre, M. Vallet-Regí, M. Sebban, F. Taulelle and G. Férey, *Angew. Chem., Int. Ed.*, 2006, **45**, 5974–5978.